Surface and electron structure of the 6H-SiC(0001)-(3×3) surface and ultrathin Ag films on Si(111) and Si(001)

V.A. Gasparov

Institute of Solid State Physics RAS, Chernogolovka, Moscow district 142432, Russian Federation
E-mail: vgasparo@issp.ac.ru

Surface topographic (LEED, STM) and spectroscopic (ARUPS, XPS, STS) studies have been performed on the Si-terminated 6H-SiC(0001)-(3×3) surface and Ag superstructures and ultrathin films on Si(001) and Si(111) surfaces, using a scanning tunneling microscope (STM) in ultrahigh vacuum. Our results confirm that a 2D epitaxial metal growth is favored on Si(001) at low temperatures and a solid, two-domain Ag(111) film has been achieved at coverage's as low as 10 ML. We have found that the films reveal a morphology with 3-dimensional features and with well defined honeycomb structure in between. An atomically flat Si(111)/Ag-($\sqrt{3}\times\sqrt{3}$)R30° surface has been modified by use of a scanning tunneling microscope (STM) in ultrahigh vacuum (UHV). High quality 6H-SiC(0001)-(3×3) and Si(111)-Ag($\sqrt{3}\times\sqrt{3}$)R30° over structures have been prepared and studied by means of ARUPS, XPS and LEED. The local density of states proportional to the normalized differential conductivity $(dI/dV)/(I/V)$ vs V spectra show a distinct bands of empty (–0.6 eV) and filled (0.65 eV) sites separated by 1.2 eV, for both areas. The results support a Mott–Hubbard-type model as used for the calculation of the density of states of 6H-SiC(0001)-(3×3) surface with Hubbard gap 1 eV.

1. Introduction

The considerable change of our knowledge about the physics of electrons in quantum size systems was obtained within the last two decades or so, due to investigations of self-organized structures on semiconductors: surface phases (SP), ultrathin films like graphene, etc., metallic clusters and terrace films on vicinal surfaces (see review papers [1–3] and references in [4–10]). These structures can be used as new low-dimensional quantum systems, whose electron transport property study at low temperatures become recently a very important challenge of surface physics. The character of these features suggests that these structures, especially graphene films, are considered to be a possible candidate to replace silicon in electronic devices. Thus, if suitable methods were developed in order to prepare these structures, it would be possible to combine the advantages of these structures to achieve high mobility new devices.

High degrees of order and homogeneity of these films and knowledge about their structural properties are very crucial for these studies. Such systems must be high-purity ultrathin single-crystal films of metals with atomically flat surfaces and only a few atomic layers thickness with atomically flat surfaces, self-assembled chain-like terrace films on vicinal surface, or metallic islands with well defined sizes. In order to make electrical transport measurements, the substrate has to be insulating. SiC and Si are very suitable substrates, because atomically flat Si(111) and Si(100) surfaces can be easily prepared and these substrates become almost insulating at low temperatures due to freezing of carriers. It is clear, that prior to the preparation of thin film quantum devices, the detailed structural information on formation of the metal–semiconductor interfaces is necessary. Although, these investigations are a topic of strong interest in surface science during many years, new very exciting results have been obtained last time, which

makes this field a very important challenge of surface physics and nanoelectronics.

The Ag/Si system has been considered as a model system for the study of ultrathin films and surface phases due to Ag inert nature. However, this system has a complex phase diagram above room temperature in which coverage and temperature play an important role [2–4,6–10]. In particular, the Ag/Si(111) and Ag/Si(001) surfaces has been studied by almost every surface analysis techniques and many different surface phases has been observed for monolayer and submonolayer coverage's [2–4]. At larger coverage's however, the metals form 3D-cluster structure at RT due to large lattice mismatch with Si: in general all metals has lattice parameter less than for a semiconductors. Therefore, the heteroepitaxial growth of the metal films on semiconductors is a topic of great fundamental and technological interest in order to explore the potential of quantum devices.

The morphology and electron structure of SiC surfaces have been studied extensively due to a unique combination of exceptional properties such as wide band-gap, high-temperature semiconducting properties and polytype structure, which provides an insulating substrate at temperatures below 50 K [5]. The cubic zinc-blende polytype β-phase (3C) has attracted particular attention, while the hexagonal α phase (e.g. 4H and 6H polytypes) was recently investigated too. The low energy electron diffraction (LEED) and band structure of these superstructures was observed to be identical on both 3C-SiC(111) and 6H-SiC(0001) surfaces because the respective stacking sequences are the same down to at least four layers from the surface. It has been demonstrated that annealing of SiC(0001) in UHV at 800–1000 °C in a flux of Si atoms results into a (3×3) reconstruction, which turns into a ($\sqrt{3}\times\sqrt{3}$) R30^o superstructure upon further annealing without Si flux. Further heating at 1150 °C leads to ($6\sqrt{3}\times6\sqrt{3}$) LEED patterns, which was shown from STM consisting of a mixture of (6×6), (5×5) and ($\sqrt{3}\times\sqrt{3}$) superstructures [13]. Finally graphene films are developed at 1400 °C [11,14].

Although the band structure calculations in the framework of the density-functional theory and local-density approximation predicted metallic behavior for (3×3) and ($\sqrt{3}\times\sqrt{3}$) R30^o superstructures, no density of states has been found at the Fermi level by ultraviolet photoemission (UPS), and **k**-vector resolved inverse photoemission spectroscopy (KRIPES) investigations. More recent calculations demonstrated that a Mott-Hubbard insulating ground state is a realistic scenario to solve this problem [5]. This model predicts that the energy structure of 6H-SiC(0001) (3×3) and ($\sqrt{3}\times\sqrt{3}$) superstructures consist of a filled and an empty band separated by a Hubbard gap of 1.6 eV and 1 eV, respectively. Indeed, the scanning tunneling spectroscopy (STS) data of the 6H-SiC(0001) ($\sqrt{3}\times\sqrt{3}$) surface indicated a gap of 2.0 eV, in good agreement with ARUPS and KRIPES experiments (2.3 eV) and theoretical

calculations employing a two-dimensional Hubbard model (1.6 eV) [5]. However, the electron structure of the 6H-SiC(0001) (3×3) reconstruction is not clear. While the ARUPS spectra at low energy indicated a filled band at — 0.65 eV, there is controversy regarding the empty surface state.

In this paper we present a review of our data on the morphology and band structure of Ag/Si and 6H-SiC(0001) surfaces performed by UPS, XPS, LEED, STM and STS on the (3×3), ($\sqrt{3}\times\sqrt{3}$) R30^o and ($6\sqrt{3}\times6\sqrt{3}$) superstructure of the Si-terminated 6H-SiC(0001) surface and on the low temperature growth of Ag films for both Si(001) and Si(111) surfaces at large coverage's. Compared to ARUPS/KRIPES experiments, STS has the advantage that a tunneling spectrum provides the information on the band structure above and below E_F at the same spatial location. Finally, the possibility of writing lines and formation of surface features (dots, mesas) onto an atomically flat Si(111)/Ag-($\sqrt{3}\times\sqrt{3}$)R30° surface by aid of STM nanopatterning will be demonstrated. We believe that these 2D electron structures hold great scientific potential.

The outline of this paper is as follows. In Sec. 2 we introduce our experimental techniques for investigating the atomic structure, electronic states, nanostructuring and electron conductivity of the surface superstructures and Ag thin films on Si. Section 3 describes the atomic and electron structures of Ag on Si(111) and Si(001) superstructures and 6H-SiC(0001) surfaces examined by these techniques, where we confirm that a 2D epitaxial metal growth is favored on Si(001) at reduced substrate temperatures and has peculiar behavior on Si(111). Section 3.3 describes surface topographic (STM), spectroscopic (STS), ARUPS, XPS and LEED studies performed on the Si-terminated 6H-SiC(0001)-(3×3) surface using a STM in ultrahigh vacuum. The Sec. 4 is devoted to the STM manipulation used to create a mounds in plus polarity and a pits in minus polarity with nanoscale sizes on Si(111)/Ag-($\sqrt{3}\times\sqrt{3}$)R30° surface. Section 6 contains our conclusions.

2. Experimental

The experiments have been performed in an UHV multi-chamber surface analytical system with a base pressure of 2·10^{-8} Pa, which allows *in-situ* preparation of the Si and SiC surfaces, Si and Ag deposition as well as characterization by means of UPS, XPS, AES, LEED and STM [4–6]. The STM is a commercial large sample type from Omicron. Electrochemically etched (2M NaOH) single crystalline W<111> and hand cut PtIr tips have been used which were outgases and flash annealed in UHV. The images were recorded at room temperature in the constant current mode at voltages ranging between –3.0 to +3.0 V and a current of 0.01–0.03 nA for SiC and at gap voltages ranging from ±0.4 V to ±1.0 V and a tunneling current of 0.1 nA for Si samples. All given voltages are referring to
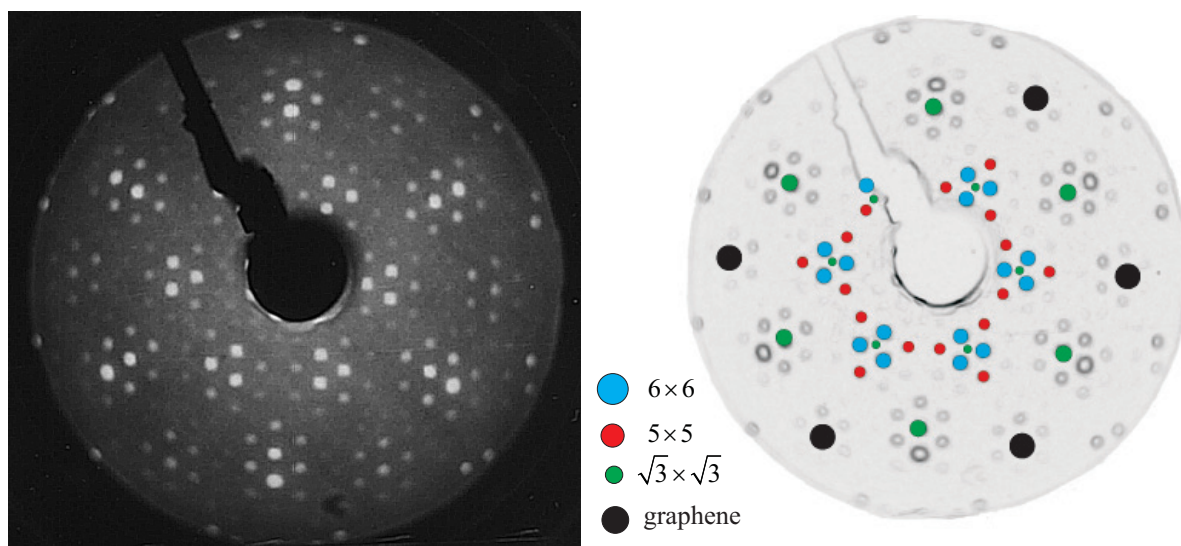
Fig. 1. (Color online) LEED patterns from 6H-SiC(0001) ($6\sqrt{3} \times 6\sqrt{3}$) reconstruction recorded at $E = 91$ eV (*a*), Trace contour from a LEED picture: different symbols shows reflections from 6×6, 5×5, $\sqrt{3} \times \sqrt{3}$ reconstructions and graphene spots (*b*).

the substrate polarity, the tip was grounded. Tunneling spectra were obtained by measuring the tunnel current *I* as a function of the voltage *V* across the tunnel junction.

The Si(111) and Si(001) samples (oriented within 0.1° to the <001> and <111> directions) were cut from commercially available Si wafers (*n*-type, 5 Ω·cm), which has been degassed in UHV by step rise of the temperature from 300 °C up to 600 °C for 12–24 h and flash annealed to a temperature of about 1200 °C to remove oxides, while maintaining a background pressure bellow $1 \cdot 10^{-7}$ Pa. Samples were fixed in a molybdenum holder and could be heated by means of electron bombardment of the rear side of the sample. All temperatures were measured by thermocouple. The STM experiments were performed at a base pressure of $5 \cdot 10^{-8}$ Pa and were showing very rough surface consisting from 3D clusters after this treatment on both samples: with native oxide layer or hydrogen terminated surface, even though a good (7×7) LEED structure have been observed. In order to obtain atomically flat surfaces an epitaxial Si film of about 10 nm thick has been grown subsequently at a temperature of 650 °C. LEED and the STM consistently verified well-ordered (7×7) and (2×1) structures on Si(111) and Si(001) samples, respectively. The Si(111)/Ag-($\sqrt{3} \times \sqrt{3}$)R30° overlayer ($\sqrt{3}$Ag/Si , hereafter) has been achieved by deposition 1 ML Ag from a filament-heated tantalum crucible at a rate of 0.02 Å/s onto Si(111)–7×7 substrates kept at 500 °C. The evaporation mass flux was monitored by a quartz-crystal microbalance. The STM showed 600 nm wide atomically flat terraces with 2D islands of Si(111)/Ag-($\sqrt{3} \times \sqrt{3}$)R30° double layer height 3.1 Å, indicating the partial second layer of Ag on the Si substrate. At both levels, atomically resolved STM images indicate the honeycomb structure, which is charac-

teristic for the Si(111)/Ag-($\sqrt{3} \times \sqrt{3}$)R30°. LEED investigations confirm the ($\sqrt{3} \times \sqrt{3}$) overstructure with sharp diffraction spots, while XPS revealed no detectable surface contamination.

In studies of clean SiC surfaces, there are important problems concerning the surface preparation. Our samples were doped (*n*-type, $N = 8 \cdot 10^{18}$ cm^{-3}) 6H-SiC(0001) single crystals cut from commercially available polished wafers from Cree Research. The samples were etched *ex-situ* in radio-frequency plasma of H_2/O_2 for 15 min at 50 Pa in a parallel plate reactor. The second step was a thermal dry-oxidation at 1200 °C for 30 min, which results in an oxide thickness of about 15 nm. Before loading into vacuum the oxide was removed by dipping into 50% HF. Samples were fixed in a molybdenum holder and could be heated by means of electron bombardment of the rear side of the sample. Clean surface superstructures were obtained from the chemically passivated (1×1) phase by heating the samples in a molecular beam Si flux at 900 °C. Depending on the exposure, ($\sqrt{3} \times \sqrt{3}$) R30° LEED patterns were observed. After sufficiently long Si exposure (5 min), sharp (3×3) LEED patterns were obtained which could be correlated to specific spectral features in ARUPS [5]. Further heating at 1150 °C without Si flux lead to ($6\sqrt{3} \times 6\sqrt{3}$) and graphene LEED patterns that is shown in Fig. 1. Subsequent annealing of the prepared structure up to 1400 °C resulted in thin graphene layers, with the layer thickness determined predominantly by the temperature [11,14]. This picture can be described by a combination of reciprocal lattice vectors from the (6×6) and (5×5) together with the reciprocal lattice vectors from the ($\sqrt{3} \times \sqrt{3}$) reconstruction and graphene films.

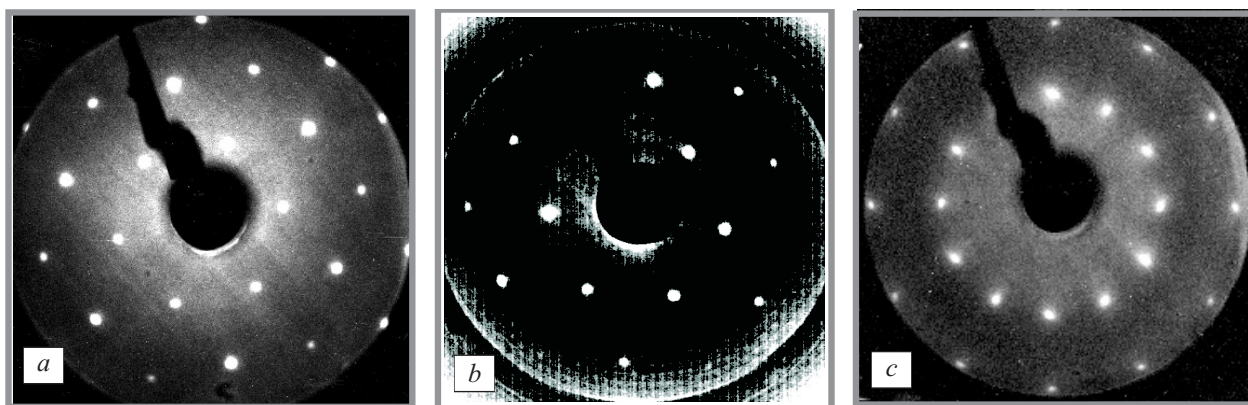*Fig. 2*. Typical LEED patterns of: $\sqrt{3}$Ag/Si surface (*a*), 5ML Ag deposition at 130 K on this surface (*b*), 10 ML Ag film evaporated at LT on Si(100)-c(2·1) surface, recorded at RT (*c*). The electron beam energies are 48 eV, 85 eV and 130 eV, respectively.

3. Results

3.1. Si(111)($\sqrt{3}\times\sqrt{3}$)Ag *surface*

The STM topography reveals large (200 nm) atomically flat regions of well ordered Si(111)7×7 phases with atomic steps in between [4]. Figure 2 shows the diffraction LEED pattern around the Si(10) diffraction spot for a $\sqrt{3}$Ag/Si surface, a 5 ML Ag film deposited at 130 K on this surface as well as for a 10 ML Ag film evaporated at LT on Si(100)-(2×1) (Fig. 2,*c*).

A large area topographic STM scan of a $\sqrt{3}$Ag/Si surface prepared at 500°C is shown in Fig. 3. In this image, reflecting the filled states of the sample, the position of $\sqrt{3}$Ag/Si islands appear as bright areas. A high-resolution filled-state STM scan recorded at RT on these islands is shown in Fig. 3,*b*. Atomically resolved STM images indicate the characteristic honeycomb structure with a low defect density. LEED as shown in Fig. 2 confirm a sharp ($\sqrt{3}\times\sqrt{3}$) structure and XPS showed no detectable surface contamination. The atomic arrangement of this well known $\sqrt{3}$Ag/Si superstructure has been solved by the honeycomb chained trimer (HCT-1) model [15].

As we can see from the Fig. 3, STM study showed wide atomically flat terraces with 2D islands of double mono atomic step height, indicating the partial second layer of $\sqrt{3}$Ag/Si on the Si substrate [4]. These non percolated terraces are connected by a non conductive wetting layer which is responsible for the percolation resitivity on this surface. The profile lines of the STM images have shown that the average height of these islands is 3.1 Å above the adatoms of the wetting layer. This is significantly larger than the Ag(111) step height of 2.36 Å. Thus formation of $\sqrt{3}$Ag/Si islands (Si trimer with Ag layer on top) at coverage of 1 ML silver showing a uniform thickness of one atomic layer was observed. The lateral size of these islands varied from 60 nm to 600 nm, indicating that once a $\sqrt{3}$Ag/Si island is formed, it starts to grow in size laterally. The 2D growth behavior of 2-layer islands is likely driven by the quantum well states [4].
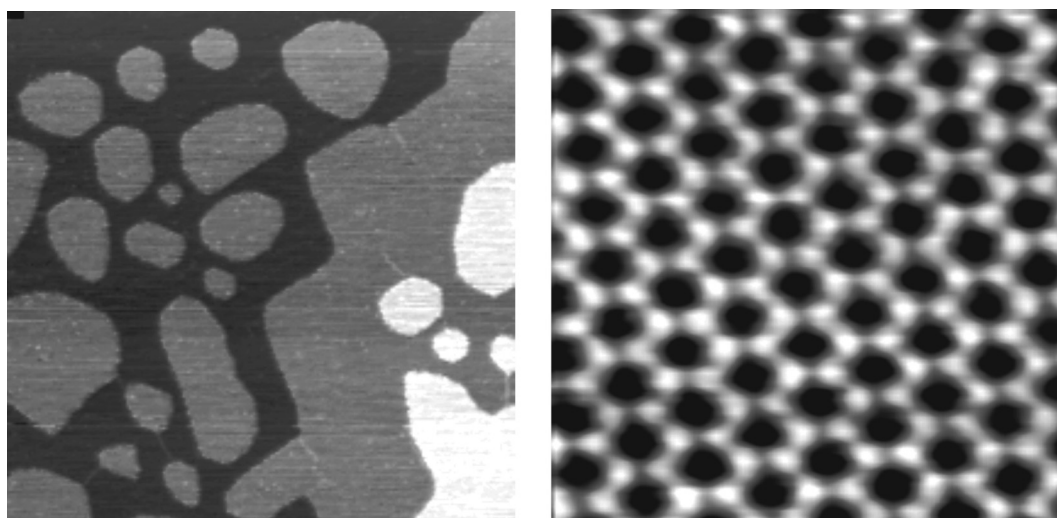

Fig. 3. (Color online) STM topographic image of $\sqrt{3}$Ag/Si at 265×265 nm (left panel) and at high resolution 12×12 nm (right panel). The images were recorded at 0.1 nA tunnel current and −0.6 V bias voltage.

In order to study the local electron structure of the $\sqrt{3}$Ag/Si surface we performed STS experiments simultaneously with STM imaging under the condition of a fixed tip-sample distance [4]. That is, a measurement of a tunneling current versus bias voltage spectrum with the STM feedback loop turned off at each point during scanning of the tip over the surface. From these spectra we can calculate the normalized differential conductivity $(dI/dV)/(I/V)$ which is proportional to the local surface density of states (LDOS) on the topographic image. As it was suggested by Stroscio et al. [16], the normalized differential conductance is proportional to the local surface density of states (LDOS), $\rho_s(eV)$ with energy eV:

$$\frac{dI/dV}{I/V} \propto \rho_s(eV) \frac{eV}{\int_0^{eV} \rho_s(E)D(E)dE}, \qquad (1)$$

where $D(E)$ is transmission probability. Thus, Eq. (1) provides direct measure of the LDOS from $(dI/dV)/(I/V)$ vs V dependence.

The corresponding normalized differential conductance, was calculated numerically from $I–V$ curves and is presented in Fig. 4. The area resolved data provide a direct measure of the spatial distribution of the local density of states (LDOS). In these figures the Fermi level corresponds to 0 V and the energy is measured from the sample voltage relative to E_F. In order to account for the singularity problem close to 0 V, where the measured current and conductance drop below the noise level, the $I–V$ curves in a plateau region were fitted simply with an exponential function according to [16]:

$$I \propto \int_0^V \exp\left(-AZ\sqrt{\phi - V}\right) dV. \qquad (2)$$

Here ϕ denotes the local tunneling barrier, A is a free parameter and Z is the sample-tip separation. In each case 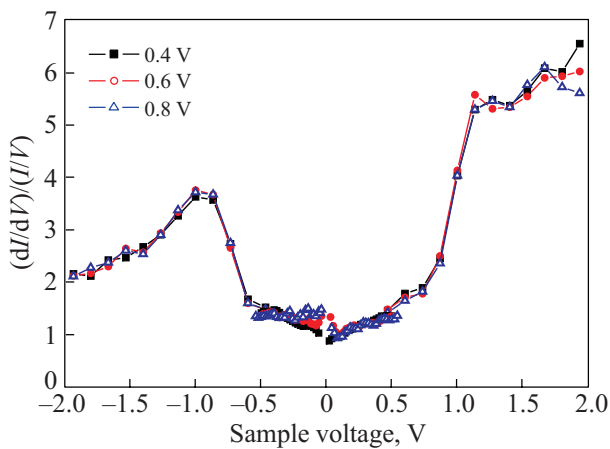these parameters have been adjusted by fitting experimen-tal $I–V$ curves for $V < 0$ and $V > 0$ separately, thereby eliminating the singularity of conductance within the band gap. The subsequent broadening of conductance produces a smoothly varying normalized conductance calculated from the experimental values of the differential ones. At high voltages outside this region and for linear $I–V$ dependencies close to E_F, the normalization quantity was numerically calculated without using Eq. (2) broadening.

The Fig. 4 shows normalized differential conductivity, as calculated numerically from the $I–V$ curves, averaging the profiles of the STM image of $\sqrt{3}$Ag/Si 2D islands. A significant feature of these dependencies is the observation of two maxima at −1 eV and +1 eV in the normalized differential conductance as presented in Fig. 4. The peak positions remain unchanged for different islands indicating a uniform LDOS distribution in the area where the $\sqrt{3}$Ag/Si structure is formed. Thus a semiconductor band structure of the $\sqrt{3}$Ag/Si surface with an energy gap of 2 eV is observed in contrast to 2D metallic like system as proposed in Ref. 2. Notice usual STS problem because the both measured conductance and differential one drop below the noise level close to 0 V. This is due to plateau region of the $I–V$ curves inside a gap. In order to avoid this problem, we fitted I vs V dependence close to zero voltage and calculated $(dI/dV)/(I/V)$ from this fitted curves, that is what is shown in Fig. 4. Note also, that metallic behavior will produce linear I vs V dependence, while we have a plateau [4].

When comparing the normalized conductance STS curves with UPS data, we see similarities for the filled states. As in STS experiments a sharp reduction of the DOS at binding energy $E - E_F = -1$ eV can be seen in the PE spectra of $\sqrt{3}$Ag/Si surface in Fig. 5. These UPS data at −1 eV are in a good agreement with S_2 states observed in

Fig. 4. (Color online) The normalized differential conductance $(dI/dV)/(I/V)$ vs V STS spectra from the I vs V data measured for different tip-surface separations for the $\sqrt{3}$Ag/Si surface.
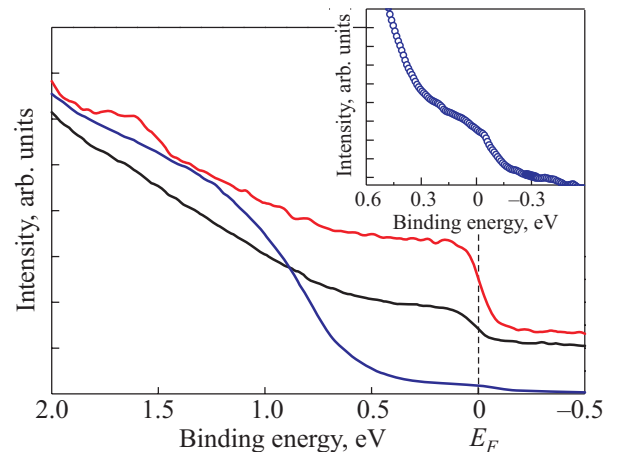

Fig. 5. (Color online) The angle-integrated valence band UP spectra for $\sqrt{3}$Ag/Si surfaces and for a bulk Ag single crystal (upper curve). The lower spectrum was measured on a regular $\sqrt{3}$Ag/Si surface while the middle curve was obtained from 5 ML Ag film on $\sqrt{3}$Ag/Si surface. The photon source was He I ($h\nu = 21.2$ eV). Inset shows extended part PE spectra close to E_F for $\sqrt{3}$Ag/Si surface.

ARUPS experiments [2]. We did not find metallic S_1 states in our STS studies likely due to the highly local character of the STS experiments performed only on top of $\sqrt{3}$Ag/Si islands, in contrast to sample averaged ARUPS or UPS data. This suggests that the surface band structure of $\sqrt{3}$Ag/Si surface is inherently semiconducting and metallic behavior observed from ARUPS may be due to Ag excess on top. From the comparison to the bulk Ag PE spectrum and a 5 ML Ag film evaporated at 130 K on $\sqrt{3}$Ag/Si , we can see a quite clear Fermi edge for the LT prepared films being consistent with the metallic character. Subsequent annealing of the LT prepared structure up to 500°C resulted in the same spectra. At the same time, the $\sqrt{3}$Ag/Si surface exhibit clear semiconducting behavior with the same gap for the filled states as in STS experiments. Apparently, the tiny Fermi edge formation is due to Ag excess on top of $\sqrt{3}$Ag/Si islands (see inset to the Fig. 5).

It is currently believed that the $\sqrt{3}$Ag/Si surface is arranged according to the HCT-1 model [15]. In this model the top Ag and uppermost Si atoms form trimers on the surface. However, recently, different versions of this model have been suggested for the LT phase of $\sqrt{3}$Ag/Si surface with a slightly asymmetric modification of the Ag trimers described by the in equivalent triangle (IET) model (see references in [4]). Accordingly cooling from RT to LT should provoke a phase transition from HCT-1 to the IET surface. However, recent LT ARPES studies of Uhrberg *et al.* of the $\sqrt{3}$Ag/Si surface did not find any splitting at low temperatures [17]. Therefore, it was concluded that the HCT-1 model for the $\sqrt{3}$Ag/Si surface is the most reasonable one.

Also it was proposed from ARPES studies that the $\sqrt{3}$Ag/Si surface is intrinsically metallic [2,3]. Some indication of a partial surface metallization can be seen from our UPS data in the inset of Fig. 5 indeed. However, recent ARPES studies [17,18] have shown that there is a significant effect of additional Ag atoms on the surface electronic structure near the Fermi level. Although the difference between UPS and STS data is clear, we have to point out that islands structure of $\sqrt{3}$Ag/Si surface may manifest the photoemission data, while the STS data in Fig. 4 are taken from well defined regular $\sqrt{3}$Ag/Si surface sites. Thus we believe that the tiny indication of the Fermi edge observed in Fig. 5 is due to additional Ag atoms adsorbed on top of $\sqrt{3}$Ag/Si surface and the pure $\sqrt{3}$Ag/Si surface is semiconducting according to our STS data (see Fig. 4). Another important result of our UPS data is the observation of a clear metallic behavior of the 5 ML Ag film on top of the $\sqrt{3}$Ag/Si surface. In order to decide whether these films are solid, we performed XPS studies with the same light incident angle of 20° with respect to the surface normal as in the UPS experiments [4]. We found that these spectra show peaks that can be related to the original components of Ag and Si of the surface atoms with no indication of

contaminations. After the deposition of 5 ML Ag at 130 K the XPS data show that the Si 2*p*-peaks almost disappear, indicating that the Ag films on the $\sqrt{3}$Ag/Si substrate are almost solid. Thus, according to our LEED, UPS and XPS studies, we may conclude that the low temperature evaporation of 5 ML Ag films on $\sqrt{3}$Ag/Si leads to peculiar growth of metallic solid films.

In order to confirm or not this unusual conclusion we performed STM studies of the 5 ML Ag films evaporated at LT on $\sqrt{3}$Ag/Si . We first prepared the $\sqrt{3}$Ag/Si phase by high temperature Ag deposition. Then we subjected the $\sqrt{3}$Ag/Si to LT (130 K) deposition of a 2–5 ML of Ag on top of this phase in order to achieve 2D films. Figure 6 shows an STM image of the $\sqrt{3}$Ag/Si surface after deposition of 5 ML of Ag films at 130 K and subsequently warmed up to RT. Contrary to the LEED and XPS data, we found that this film consists of rather narrow and large Ag islands with atomically flat Ag(111) top facets in between. The typical width of these islands is 50 nm and the height is about 4 nm.

The area between these islands retains atomically flat $\sqrt{3}$Ag/Si terraces with a width of about 200 nm. The symmetry and orientation of the flat terraces between these islands with clear honeycomb geometry suggest a $\sqrt{3}$Ag/Si structure in agreement with the HCT-1 model [15]. This

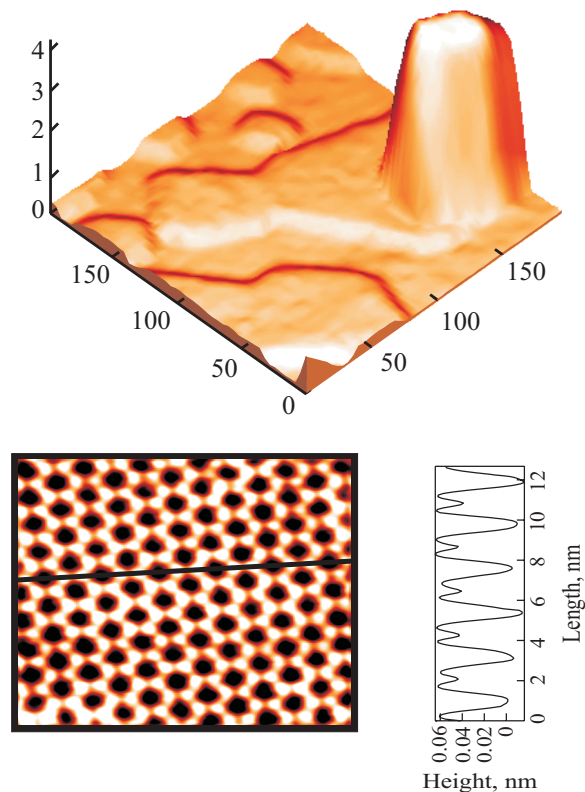*Fig. 6.* (Color online) Filled state STM image from 5 ML Ag deposited at LT onto $\sqrt{3}$Ag/Si showing large Ag islands with $\sqrt{3}$Ag/Si areas in between (top panel). The atomically resolved STM image recorded in between the Ag islands (9×12 nm) indicates the $\sqrt{3}$Ag/Si structure (bottom panel).

conclusion is confirmed by the high resolution STM image with the profile presented in the lower panel of the Fig. 6. This image reveals hexagonal features consisting of six protrusions related to Ag trimers on top while the dark spots apparently are related to the Si trimers.

The observed Ag island distribution may be explained by diffusion of the Ag atoms from the wetting layer across the surface while warming up to RT. Apparently, the surface free energy drives the system into the energetically favorable configuration characterized by larger isolated Ag 3D crystallites. The Ag atoms migrate to the top of existing islands during warm up to RT thus increasing their height and preserving their regular shape. A similar behavior has been observed for the transfer of Pb from the wetting layer of √3Pb/Si surface to the seven layer islands during annealing from 115 K to 180 K by low temperature STM experiments [19]. Therefore, additional LT STM studies of LT prepared Ag films on √3Ag/Si substrates with different coverage are needed in order to elucidate the exact atomic structure of these films.

3.2. Ag(111) *films on* Si(001)

First we prepared the Si(100)-(2×1) superstructure by high temperature homo epitaxy of Si as described for the Si(111) surface. We then subjected the Si(100)-(2×1) surface to the deposition of 5–20 ML Ag films at 130 K. Figure 2,*c* illustrates the LEED pattern from the 10 ML Ag film after annealing to RT. From first glance the LEED pattern are very peculiar. The zero spot is surrounded by 12 first-order spots and 12 second-order ones. However, a closer analysis can easily explain these pattern as a superposition of the twinned domains of Ag(111) surface, i.e. a Ag(111) LEED pattern rotated by 90° with respect to each other [4]. The spots are elongated in two perpendicular <110> directions indicating superposition of two Ag domains rotated by 90°.

The morphology of this 10 ML film was studied by STM too [4]. The cornered shape of the step edge confirms the in-plane orientation of the Ag grains as deduced from the LEED pattern. The reason for this observation can be understood by comparing the Ag and Si lattices. The Si/Ag interface exhibits an almost exactly 4/3 mismatch ($a_{Si} = 0.5431$ nm and $a_{Ag} = 0.4086$ nm), thus the distance between three Si atoms matches the distance between 4 Ag atoms [4]. According to a recent reports ultra thin Ag(111) films are epitaxially formed by deposition up to 40 ML of Ag at LT (< 130 K) on Si(001) surfaces followed by post annealing to RT [4].

In order to understand whether these films are metallic we studied the electronic states on this surface by angle integrated UPS. Figure 7 shows the UPE spectra for the Si(001)-(2×1) surface and the 10 ML Ag film grown on it at 130 K and annealed to RT. The drastic change of the electronic structure of the Si(001) surface induced by the Ag film is obvious. The spectral shape of the valence band
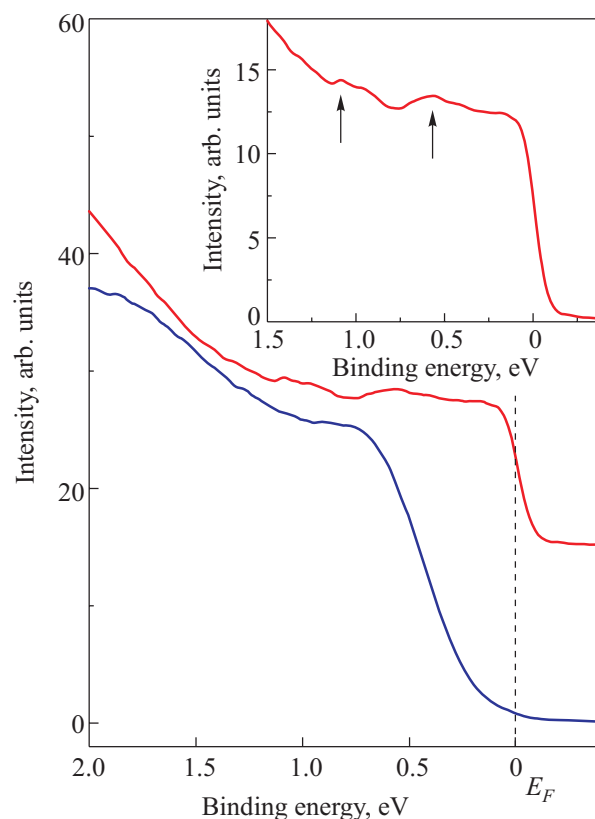

Fig. 7. (Color online) The angle-integrated valence band PE spectra obtained at RT from a Si(100)-(2×1) surface (bottom curve) and from 10 ML Ag film (top curve) deposited on it at 130 K. Inset shows extended part of PE spectra close to E_F for this film.

UPE spectra from the 10 ML film is similar to those of the Ag deposited on top of √3Ag/Si and the Ag single crystal presented in Fig. 5 indicating metallic state formation. The formation of such states for the LT deposited films is consistent with our STM data in Fig. 7 and the LEED results shown in Fig. 2,*c*.

Several small peaks at binding energies of 1.2 and 0.6 eV below the Fermi edge appear which may be assigned to quantum well states (QWS) [4]. These states are due to energy quantization phenomena of confining electrons in a spatially narrow potential well produced by thin film. In this case the thickness of atomically flat film has to be an integer of the Fermi wavelength. The thickness of the 10 ML Ag film is about 2.36 nm which seems to be enough to realize the quantum confinement of carriers in the film. Thus our observation of these QW states is another proof about 2D metallic character of the Ag films on the Si(100)–2×1 surface.

Finally we can conclude that the Ag film deposited at LT on Si(001)-c(2×1) becomes metallic with a 2D twinned Ag film after annealing to RT due to the integer-ratio lattice mismatch of 3/4 [4]. At the same time Ag grows at RT on Si(100)–2×1 clean surface in island-growth mode up to 40 ML coverage [4].

3.3. Resistivity of Ag(111) films on Si(001)

Our typical result of conductance versus temperature measurements of a Si(100)–2×1 substrates and a 4 ML Ag film on it deposited at 45 K are shown in Fig. 8 [4]. The conductance of the clean substrate sharply drops in the temperature range from about 170 K to 45 K monotonously due to freezing out of the number of carriers. In turn, the resistance drops in one order of magnitude after 4 ML Ag film deposition. Thus we can account for the conductivity of the Ag film by subtracting the substrate conductance. The result is shown by triangles and displays a completely different behavior as compared to the substrate. The film conductance has a maximum at 140 K and then drops at higher temperatures. Note however, that the data precision is rather low beyond this maximum due of the small conductance change with respect to the substrate. In contrast to the expected metallic behavior the conductance sharply decreases below the maximum but is not reaching zero as the substrate.

The observed difference in σ(T) is obviously due to the different conduction mechanisms in the film and the substrate. For the weak localization and low temperature region a logarithmic temperature dependence of the conductance $\sigma(T) \propto \log(T)$ is expected. On the other side, according to variable range hopping conductivity within a band of localized states, $\sigma(T) \propto \exp(T_0/T)^{1/3}$ could be expected [20]. However, we could not fit the data quantitatively with any one of these laws. A reasonably fit was obtained for a modified variable range hopping conductivity with a non-zero residual conductance σ(0):

$$\sigma(T) = \sigma(0) + \sigma_1 \cdot \exp(-T_0/T)^{1/3}. \qquad (3)$$

The fit with Eq. (3) is shown in Fig. 8 as a solid line through the Ag film conductance data. Thus we can speculate that the residual conductance might be due to in grain
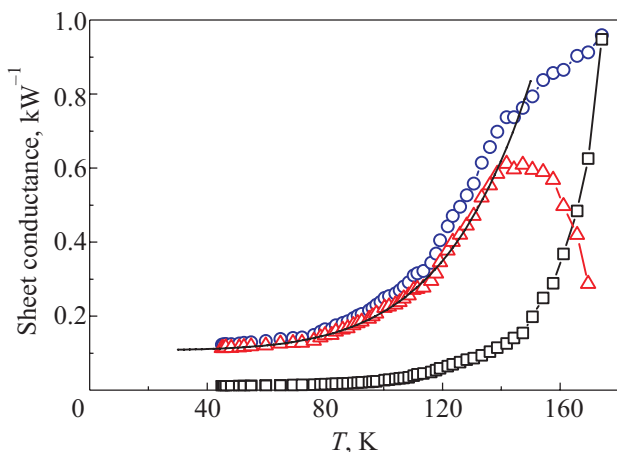

Fig. 8. (Color online) The conductance versus temperature dependencies for a 4 ML Ag film (circles) deposited at 45 K on Si(100) and for the bare Si(100) substrate (squares). The triangles show σ vs T for the Ag film after substrate subtraction.

conductance while the second term is due to the conductance inside a grain blocked by the energy of charging up a grain. The grain boundaries are large angle boundaries within 90 degrees of in-plane rotation according to the structure model [4]. So far it is not clear whether this or other theoretical model can provide a satisfactory agreement with the observed temperature dependence of conductivity. We believe that additional studies for thicker films are needed.

The relation between the surface structure of metal layers on top of Si(111) and their electrical conductivity has been emphasized in a number of papers (see [2–10]). Herein a new type of conduction through 2D electron systems localized in the surface-state bands was proposed. Although the results are really spectacular, there are conductivity problems. Simple estimations of surface conductivity as the difference from sample conductivity with superstructure minus substrate conductivity, shows that the changes observed can be due to too highly conductive surface layer with a conductivity σ_{Ag} of metallic silver if we consider one mono-layer thickness.

Apparently, the sharp metastable resistivity drop produced by metal evaporation at room temperature is caused by the adsorption-induced changes in surface states and band bending beneath the surface rather than the conductance through the surface-state bands. Notice also, that recently the rapid drop of resistance was observed in similar experiments only after the critical coverage of 1–3 ML [21], while earlier [2] this drop took place at sub monolayer coverage. This phenomenon was associated with an island coalescence and formation of percolation paths for electrical conduction [21]. Indeed, our data as shown in Fig. 3, indicate that two layer thick $\sqrt{3}$Ag/Si islands occur with large separations among them rather than the formation of a continuous 2D electron system localized in surface bands.

Our goal is the preparation of a real 2D metallic conducting layer on silicon with enhanced mobility and we believe that Ag films on Si(100) is one of the best candidate for this scenario.

3.4. STS/STM on the 6H-SiC(0001) surface

Figure 9,a shows topographic images of a 6H-SiC(0001) (3×3) reconstructed surface at the atomic level with a rather high density of defects, which are presumably due to missing adatoms. Some "black sites" in a (3×3) structure occur as a combination of several vacancies constituting a tetrahedral cluster. While there is significant polarity dependence in the appearance of some defects for empty and filled states [5], the positions of the most hexagonal array of bright protrusions of the (3×3) reconstruction are identical for both states. The unit length is 1.56 nm and the corrugation along the closely packed atomic row is about 1 nm. The corresponding tunneling spectra, current I vs. bias voltage V curves, recorded on the topographic image,
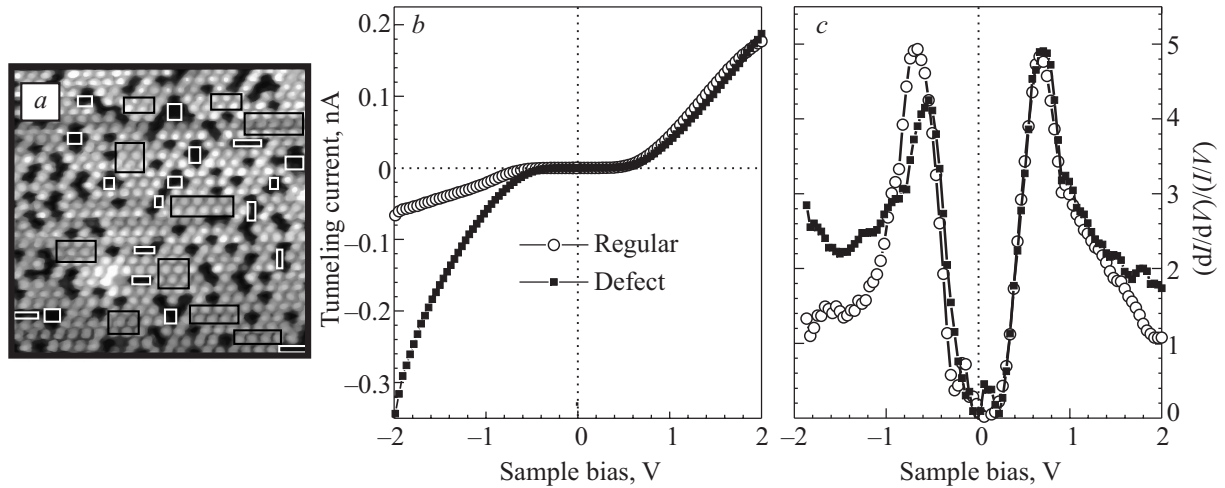
Fig. 9. (Color online) 40×40 nm STM image with a line scan of the 6H-SiC(0001) 3×3 reconstruction (*a*). *I–V* dependencies for the defect (black points) and regular (open points) surface sites (*b*). Ratio of differential to total conductivity versus sample voltage for defect and regular surface sites (*c*).

are presented in Fig. 9,*b*. The lower curve corresponds to the data averaged on the surface areas of the defect positions and the upper one is averaged for regular (3×3) surface sites. A significant larger tunneling current appears for defect sites at negative sample bias, as seen by dark dots in Fig. 9,*a*, while the regular surface sites exhibit about one order of magnitude less conductance for filled states and the same one for empty states. Note the n-type asymmetry of the *I–V* curve for defect states [5] and a rather symmetric one for regular surface sites.

When comparing the normalized conductance curves of defect surface sites with regular (3×3) ones as presented in Fig. 2,*c*, we see similarities in normalized curves for both filled and empty states, while a large difference in the total conductance for filled states occur. This implies small variations in the LDOS in the vicinity of defects. Theoretical models [5] share that they assume an adlayer Si with Si tetramer on top. Therefore, the tunneling current arises from Si layers for both defect and regular surfaces, which may be the reason for small variations in the LDOS between regular and defect surface parts. Though the origin of these defects is not completely clear at the moment, one might conclude from the data of Fig. 9,*c* that the surface band gap on the defect and regular surface is opened.

Whether this result is consistent with the band structure for 6H-SiC (0001) (3×3) reconstruction we can see from comparison of the ARUPS and KRIPES spectra [5,22,23] recorded at normal ultraviolet and electron beam incidence. The ARUPS spectra at low energy are dominated by a feature at −0.65 eV with a small dispersion originating from the emission of a filled surface state [5]. The energy of the former surface state is in good agreement with two features at −0.5 eV and −0.65 eV of the normalized differential conductance for filled states as presented in Fig. 9,*c*. While there is no counterpart in the KRIPES data of Them-

lin et al. [22] for the empty surface state at 0.7 eV, a similar surface state was observed by Johansson et al. at 0.5 eV above E_F [23]. So it appears that the surface states identified by our STS studies are in good agreement to the results of ARUPS and recent KRIPES experiments.

According to [5], the 6H-SiC(0001) (3×3) reconstruction is associated with more than one monolayer of adsorbed Si tetramers on the Si adlayer, while for the 6H-SiC(0001) ($\sqrt{3}\times\sqrt{3}$) R30° reconstruction most models assume a Si coverage of 1/3 ML on top of a Si-terminated surface. As was stated above, the density functional theory and local-density approximation predicted metallic behavior for both superstructures, respectively [5]. However, as recently proposed [5], the electron structure of these superstructures could be described by a Hubbard hamiltonian including an intrinsic Coulomb interaction between two electrons on the same adatom. The correlation effects split the one-electron band into two bands separated by a Hubbard gap of 1.6 eV for the ($\sqrt{3}\times\sqrt{3}$)R30° and a smaller gap, 1 eV, for the (3×3) overstructure, respectively [5]. The distinct bands of empty and filled states, separated by 2.0 eV gap were observed in STS experiments for ($\sqrt{3}\times\sqrt{3}$) R30°, while for (3×3) this gap should be about half of this value. Indeed, the corresponding gap 1.2 eV for the defect and 1.35 eV for the regular surface sites observed on Fig. 9,*c* are in a good agreement to the theoretical prediction of a Hubbard gap with a value of 1 eV [5].

Figure 10 displays a series of normalized $(dI/dV)/(I/V)$ curves averaged for regular (3×3) surface sites as shown in Fig. 9,*c* and for (5×5) reconstructions determined from STM. Though there is a good agreement of our STS data to both ARUPS/KRIPES experiments and theoretical predictions, the regular (5×5) surface sites revealed an featureless $(dI/dV)/(I/V) \approx 1$ vs. V dependences, close to Fermi level ($V > −0.6$ eV). This ohmic behavior is extended up to 3 V
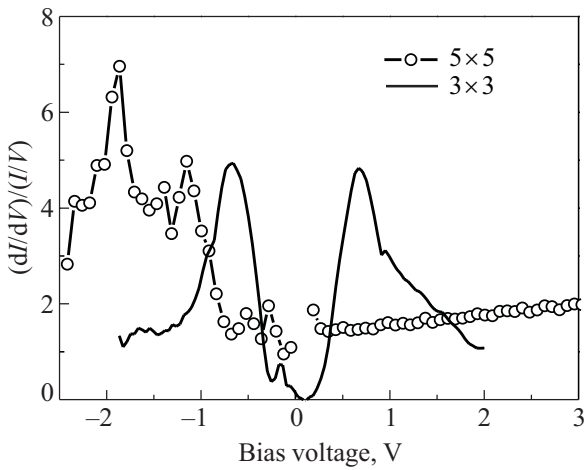
Fig. 10. The ratio of the differential-to-total conductivity vs bias voltage for the (5×5) and (3×3) reconstructions.

for positive voltages and is a fingerprint for metal-vacuum-metal tunneling. These results thereby support a breakdown of a Mott-Hubbard-type model for (5×5) reconstruction as used for the calculation of the density of states for $(\sqrt{3}\times\sqrt{3})$ and (3×3) reconstructions, and call for extended electron structure investigations.

We emphasize that the normalization procedure from Eq. (1) is an approximation, which can produce some virtual features, while the existence or absence of the states in a band gap is quite reliably determined [5]. Actually, different effects of the STM tip on the surface are known, like as a "spreading resistance" in the transport of carriers to/from the localized surface states at a relatively large current density, etc. [5]. But in any case it should show up just as additional features at a high bias or current, while none of these effects is known to produce a linear *I–V* dependence. The tip-induced development of a "metallic" behavior we observed seems to be quite distinct from the spreading resistance and band banding effects. While the exact mechanism underlying the appearance of linear *I–V* spectra for small tip-sample separations is not well understood, we believe that additional study must be performed in order to investigate band structure for (5×5) surface.

4. STM nanostructuring

Apart from the fundamental aspects discussed above, there is an increasing technological interest in nanostructured metal films on semiconductors in order to explore their potential for future nanoelectronic devices. Here, we present results on the STM induced formation of nanometer-scale pits and lines on a Si(111)/Ag-($\sqrt{3}\times\sqrt{3}$)R30° surface [6]. The surface modifications have been induced by applying voltage pulses to the sample ranging from –2 V to –6 V. In most cases of pit formation presented hereafter, the feedback loop was disengaged. Prior to the voltage pulse the tip was moved vertically with respect to a reference tip position s_0, which is defined by the feedback setting of the gap distance at +1.0 V and 0.1 nA. The pulse

duration time varied between 10 ms and 100 ms. Lines have been written by moving the tip laterally at an elevated voltage and current, while maintaining the feedback loop. The typical scan speed was in the range of 10–20 nm/s.

An example of pit formation onto a 2D island (see Fig. 3) of the $\sqrt{3}$Ag/Si layer is shown in Fig. 11. The image has been recorded after applying six voltage pulses, ranging from –3.0 V to –4.2 V — in 0.3 V steps — with a disengaged feedback loop and the tip approached by 1.3 Å with respect to the reference distance s_0 (hereafter $\Delta s = -1.3$ Å). The pits appear with a rather sharp boundary and no excess material was observed, which indicates that the atoms have been extracted from the surface and are collected on the tip. This is confirmed by the formation of round shape mounds on the surface after positive voltage polarity pulses, which apparently leads to a re-deposition of collected Ag atoms [6]. The size of these mounds is continuously decreased with the number of pulses before a complete cleaning of the tip after five or seven pulses occur due to an Ag atom supply limit effect. In this way the *W* tip could be conditioned for the pit formation process with a fairly good reproducibility.

From Fig. 11 it can be seen that the lateral size and depth (see profile line) of the holes increases with voltage. After repeating cycles of voltage pulses the threshold value at the tip position $s = s_0 - 1.3$ Å could be determined as

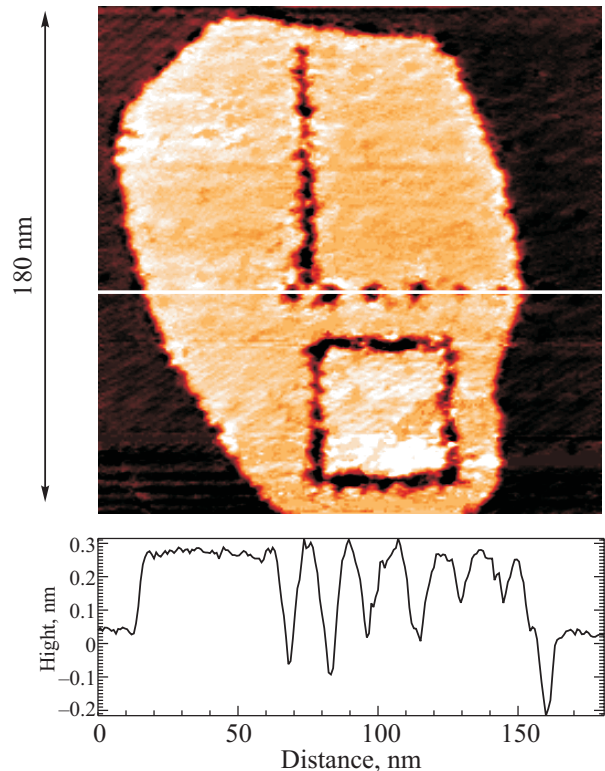*Fig. 11*. Pits formed on $\sqrt{3}$Ag/Si island at six different voltage pulses (from the right to the left): –3.0 V, –3.3 V, –3.6 V, –3.9 V, –4.2 V. The feedback loop was disengaged and the tip moved by 1.3 Å to the surface with respect to the reference distance s_0 ($\Delta s = 1.3$ Å). The pulse duration was 50 ms.

−3.0 V, which, after conditioning the tip, is reproducible within ±0.1 V. The pit size as a function of voltage has been evaluated at fixed vertical tip position with disengaged feedback loop and a pulse duration of 50 ms. As we have shown [6], the pit formation is a statistical process and depends crucially on the tip condition. Nevertheless, a rather sharp onset for atom extraction at −3.0 V can be observed, and the data clearly saturate at voltages beyond −3.6 V with a typical lateral width of around 5 nm. The profile lines in Fig. 11 show that the depth correlates with the $\sqrt{3}$Ag/Si double layer height of 3.1 Å. In some cases the hole reaches depth values of 6 Å, which indicates the extraction of Si atoms from the underlying substrate.

Occasionally the tip condition improved after Ag atom extraction and atomically resolved pictures could be recorded as shown in Fig. 12. The top presents a 28 Å wide and 50 Å long pit produced at −4.0 V and a feedback current set to 3 nA, which is surrounded by the characteristic honeycomb structure of the $\sqrt{3}$Ag/Si surface. Its shape can be regarded as a "tip-print", defined by the geometrical form of the tip. The profile line in Fig. 12,*a* shows that the pit depth is not uniform, but equals or goes beyond the $\sqrt{3}$Ag/Si double layer height labeled as d_0 in the graph. With regard to the honeycomb chained trimer HCT structure model [15] it means that Ag and Si atoms of the first double layer are extracted. In some cases an exceptionally good tip condition allowed even selective top layer Ag atom removal for voltage pulses slightly above the threshold value (see Fig. 12,*b*). According to the HCT model, the induced defect is characterized by a missing Ag trimer. Its original position is indicated by the intersecting point of the three honeycomb rings, marked as dashed lines in Fig. 12,*b*. The corresponding profile line shows a depres-

sion close to 0.8 Å, which fits nicely to the Ag–Si intralayer height given by the HCT structure model.

Upon closer inspection of these images, one can find that the honeycomb atomic structure is still present at the pit border. From this morphology a surface modification based on Ag layer melting or sublimation can be ruled out. This process has been proposed for the modification of a granular 20 nm thick Ag film, where the morphology of the produced features clearly indicates a local melting [6]. However, in our case, the atoms have been removed without disturbing the periphery of the pits, which are characterized by atomically straight edges.

Surface atom removal has also been demonstrated by mechanical contact of the tip with the surface [6]. It could be speculated that this process plays a role in our case as well, in particular taking into account the thermal expansion of the tip during the voltage pulse. Since the atom extraction takes place for a wide range of s_0 values, in particular after retraction of the tip, we believe that a mechanical contact is ruled out. The thermal tip expansion could affect our results possibly after an approach of > 5 Å. However, the threshold values are well described by a linear function over the whole gap distance range, which contradicts this assumption. Moreover, in the case of mechanical tip contact the lateral size of the produced features showed almost no dependence on the bias voltage or tip displacement, which is not consistent with our data. We therefore conclude that the observed atom extraction is predominantly caused by a field evaporation process.

Arbitrary lines could be written into the $\sqrt{3}$Ag/Si layer by moving the tip laterally at an elevated voltage and current, while maintaining the feedback loop. Figure 11 shows an example of a lines and a mesa, which has been created
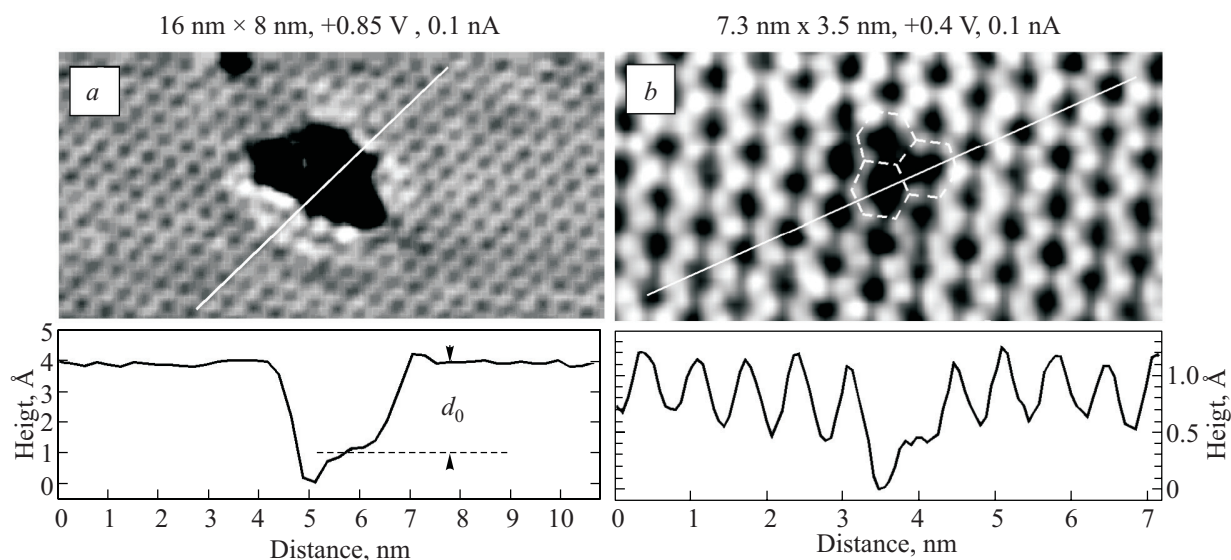

16 nm × 8 nm, +0.85 V , 0.1 nA   7.3 nm x 3.5 nm, +0.4 V, 0.1 nA

Fig. 12. Pit formation at an atomic scale: $V = -4.0$ V, $I = 3$ nA (feedback on): A 28 Å wide and 50 Å long hole is formed, which extends through the $\sqrt{3}$Ag/Si double layer. d_0 assigns the double layer height of 3.1 Å (*a*). $V = -4.4$ V, $\Delta s = -3.9$ Å (feedback off) (*b*). A silver trimer has been removed, which was originally located at the intersecting point of the three honeycomb rings marked as dashed lines. The profile line indicates selective top layer Ag atom removal. Arbitrary lines and mesa written into the $\sqrt{3}$Ag/Si layer by moving the tip laterally.

by a single patterning scan at –4.0 V and 3 nA at a scan speed of 20 nm/s. It defines a 40 nm wide mesa with a full line width ranging from 5 nm to 8 nm. At present the minimum feature size is limited by the tip quality. The process is also very sensitive to the electron dose and scan speed, which is the subject of additional experiments by using extremely sharp tips.

5. Conclusion

In summary, we have studied the electron structure and morphology of Ag overlayers on Si(111), Si(100) and on the Si-terminated 6H-SiC(0001)-(3×3) surface by means of XPS, UPS, LEED, STM and STS. Although, the XPS, UPS, LEED results show that low temperature Ag deposition favor a layer-by-layer like growth mode, a unusual $(\sqrt{3}\times\sqrt{3})$R30° structure for 4–6 ML thick Ag films deposited onto a Si(111) $(\sqrt{3}\times\sqrt{3})$R30° surface at 130 K has been observed. However, the STM study reveals a system of Ag 3D islands and atomically flat $\sqrt{3}$Ag/Si 2D terraces in between. The low temperature deposition of 10 ML Ag on Si(100)-(2×1) yields an epitaxial growth of twinned Ag(111) films with enhanced conductivity. The resistivity of these films exhibits variable range hopping conductivity at low temperatures. We conclude that the local density of states proportional to the normalized differential conductivity $(dI/dV)/(I/V)$ vs V spectra of 6H-SiC(0001)-(3×3) surface, show a distinct bands of empty (–0.6 eV) and filled (0.65 eV) sites separated by 1.2 eV, in favor of a Mott-Hubbard model. At the same time the regular 6H-SiC(0001)-(5×5) surface sites revealed an featureless $(dI/dV)/(I/V) \approx 1$ vs. V dependences, indicating metallic behavior.

We also have shown that an STM can be used to create pits at negative polarity with nanoscale sizes on a Si(111)/Ag-($\sqrt{3}\times\sqrt{3}$)R30° surface. The atomically straight edges of the pits and the linear barrier reduction with decreasing tip-surface distance are indicative for a field evaporation process. Lines and squares have been created at a scale <10 nm and a depth extending the $\sqrt{3}$Ag/Si double layer height. The proposed patterning method appears as a promising tool in order to form quantum size structures for electron transport investigations.

1. P. Moriarty, *Rep. Prog. Phys.* **64**, 297 (2001).
2. S. Hasegawa, X. Tong, S. Takeda, N. Sato, and T. Nagao, *Prog. Surf. Sci.* **60**, 89 (1999).
3. I. Matsuda and S. Hasegawa, *J. Phys.*: *Condens. Matter* **19**, 355007 (2007).
4. V.A. Gasparov and M. Riehl-Chudoba, *Surf. Sci.* **601**, 5403 (2007).
5. V.A. Gasparov, M. Riehl-Chudoba, B. Schröter, and W. Richter, *Europhys. Lett.* **51**, 527 (2000).
6. M. Riehl-Chudoba, Wo. Richter, and V.A. Gasparov, *J. Appl. Phys.* **83**, 2500 (1998).
7. V.A. Gasparov, V.V. Bondarev, and K.R. Nikolaev, *Phys. Low-Dim. Struct.* **6**, 45 (1995).
8. V.A. Gasparov and K.R. Nikolaev, *Phys. Low-Dim. Struct.* **1/2**, 53 (1995).
9. V.A. Gasparov, V.A. Grazhulis, V.V. Bondarev, T.M. Bychkova, V.G. Lifshits, and B.K. Churusov, *Solid State Commun.* **88**, 51 (1993).
10. V.A. Gasparov, V.A. Grazhulis, V.V. Bondarev, T.M. Bychkova, V.G. Lifshits, N.G. Galkin, and N.I. Plusnin, *Surf. Sci.* **292**, 298 (1993).
11. C. Berger, Z. Song, X. Li, X. Wu, N. Brown, C. Naud, D. Mayou, T. Li, J. Hass, A.N. Marchenkov, E. H. Conrad, P.N. First, and W. de Heer, *Science* **312**, 1191 (2006).
12. K.S. Novoselov, A.K. Geim, S.V. Morosov, D. Jiang, M.I. Katsnelson, I.V. Grigorieva, S.V. Dubonos, and A.A. Firsov, *Nature (London)* **438**, 197 (2005).
13. P. Mårtensson, F. Owman, and L.I. Johansson, *Phys. Status Solidi* **B202**, 501 (1997).
14. M. Riehl-Chudoba, Wo. Richter, and V.A. Gasparov, (2000, unpublished).
15. Y.G. Ding, C.T. Chan, and K.M. Ho, *Phys. Rev. Lett.* **67**, 1454 (1991); *Ibid* **69**, 2452 (1992).
16. J.A. Stroscio and R.M. Feenstra, *Scanning Tunneling Microscopy*, J.A. Stroscio and W.J. Kaiser (eds.), *Methods Exper. Phys.*, Vol. 27, Academic, New York (1993).
17. R.I.G. Uhrberg, H.M. Zhang, T. Balasubramanian, E. Landemark, and H. W. Yeom, *Phys. Rev.* **B65**, 081305(R) (2002).
18. J.N. Crain, M.C. Gallagher, J.L. McChesney, M. Bissen, and F.J. Himpsel, *Phys. Rev.* **B72**, 045312 (2005).
19. V. Yeh, M. Hupalo, E.H. Conrad, and M.C. Tringides, *Surf. Sci.* **551**, 23 (2004).
20. N.F. Mott and E.A. Davis, *Electronic Processes in Non-Crystalline Materials*, Clarendon Press, New York (1971).
21. S. Ryjkov, V.G. Lifshits, and S. Hasegawa, *e-J. Surf. Sci. Nanotechnology* **1**, 72 (2003).
22. J.-M. Themlin, I. Forbeaux, V. Langlais, H. Belkhir, and J.-M. Debever, *Europhys. Lett.* **39**, 61 (1997).
23. L.S.O. Johansson, L. Duda, M. Laurenzis, M. Krieftewirth, and B. Reihl, *Surf. Sci.* **445**, 109 (2000).